Mechanical and fracture properties of diethylene glycol bis(allyl carbonate) resins

M. Frounchi, R. P. Chaplin* and R. P. Burford
Department of Polymer Science, University of New South Wales, PO Box 1, Kensington, NSW 2033, Australia
(Received 13 April 1993; revised 22 June 1993)

Mechanical properties and fracture tests were conducted on the thermoset diethylene glycol bis(allyl carbonate). It was found that both σ_y and E increase as the testing rate increases. Crack propagation which is unstable (stick-slip) at a low loading rate changes to stable propagation as the loading rate is raised. Linear elastic fracture mechanics concepts were employed to analyse the stress intensity factors *versus* the yield stress. It is suggested that the stick-slip behaviour is due to blunting of the crack, which is controlled by the yield behaviour of the resin. It is shown that a critical stress of the order of five times the yield stress must be achieved at a critical distance ahead of the crack tip. Fracture surfaces were analysed using scanning electron microscopy and optical microscopy. No indication of crazing was detected.

(Keywords: fracture; compressive yield stress; morphology)

INTRODUCTION

Diethylene glycol bis(allyl carbonate), commonly known as allyl diglycol carbonate or ADC resin, is a highly successful commercial resin used in applications where high optical transparency, low density, acceptable surface hardness and fracture toughness are important. Although ADC resin has satisfactory impact strength for many practical applications, it is notch sensitive and some applications would be enhanced if the impact strength could be improved. In this paper we present a series of comparative studies on the fracture behaviour of ADC resin and discuss the stress-relieving mechanisms that operate in this material.

EXPERIMENTAL

ADC was polymerized as flat sheets approximately 3.3 mm thick. The monomer, after oxygen removal and the addition of 3% w/w anhydrous benzoyl peroxide, was added to a flat sheet mould. This was then placed in an oven in which the temperature was slowly increased from 50 to 100°C over a period of 21 h. The cure profile was based on that used by Stevens *et al.*[1], with 10°C being added to each step to take into account the higher decomposition temperature of the initiator used. After polymerization the ADC sample was then removed from the mould and annealed at 110°C for 2 h. This procedure ensured a monomer conversion as close as possible to 100%, as determined by density measurements and the intensity of the allyl group overtone band at 6130 cm^{-1}.

Young's flexure modulus determination

The 3.3 mm sheets of cast resin were cut into rectangular plates (14 × 80 mm). The test span was 60 mm. The flexure modulus of the resin was determined in three-point bending using an Instron 1122 at different crosshead speeds according to ASTM D-790.

Yield stress measurement

Cylindrical specimens, 10 mm long and 5 mm in diameter, were used for the determination of the compressive yield stress σ_y. Tests were carried out in uniaxial compression between polished, lubricated steel plates at various crosshead speeds at 20°C.

Fracture

Double torsion testing. Crack propagation was studied using the double torsion (DT) testing geometry. The DT test is particularly useful for crack propagation studies since there is a linear compliance variation with crack length, i.e. dc/da is constant over the entire crack length. The linear compliance relationship is shown in *Figure 1* for the ADC samples. This geometry allows good control of crack propagation ('stable geometry'). The stress intensity factor K_c is given by

$$K_c = PW_m\left[\frac{3(1+\nu)}{Wt^3t_n}\right]^{1/2} \quad (1)$$

where W_m is the moment arm, P is the applied load, ν is Poisson's ratio (assumed to be 0.35), W is the specimen width, t is the specimen thickness and t_n is the thickness of the specimen in the notch plane[2]. The specimens were cut in the form of 3.7 × 30 × 60 mm rectangular plates from cast sheets. A 'V'-shaped groove about 1.2 mm deep was made along the centre line. Samples were notched at one end and a sharp blade was run along the sample from the notch tip. The DT specimens were tested in the Instron machine under compressive loadings at different crosshead speeds.

* To whom correspondence should be addressed

0032-3861/94/04/0752–06

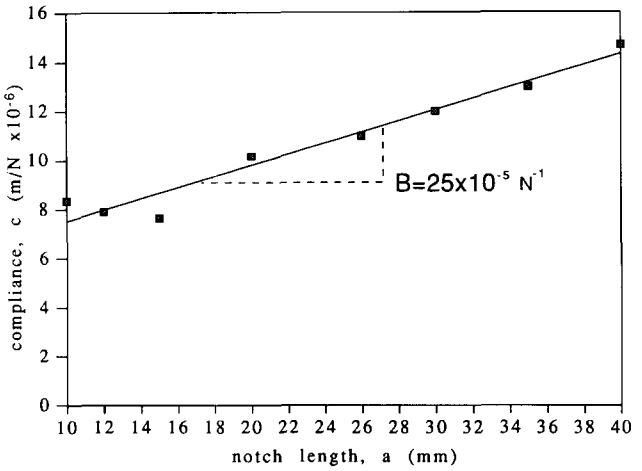

Figure 1 Compliance calibration line of the double torsion test specimen geometry for ADC

Single-edge notch bend (SENB) tests. SENB test specimens (3.7 × 14 × 60 mm) were notched with a razor blade and tested at different crosshead speeds. The notch was made through the width of the specimen with the notch length in the range $0.4 < a/W < 0.5$. The fracture stress intensity K_c was calculated using the method reported by William and Srawley[3].

Single-edge notch tensile (SENT) tests and simple tensile tests. SENT test pieces (3.3 × 12 × 120 mm) were notched with a sharp blade with the notch being made through the thickness of the sample. The notch length again was in the range $0.4 < a/W < 0.5$. The samples were tested at a crosshead speed of 1 mm min^{-1}. K_c was calculated using the method reported by William and Srawley[3].

Impact tests

Test pieces (4 × 12 × 70 mm) were notched with a sharp blade as described for the SENB test pieces. Samples were impacted at room temperature in three-point bending over a span of 40 mm using a Zeith Charpy impact tester. The velocity of the hammer at impact was 2.93 m s^{-1}. The critical energy release rate G_c was calculated using the method reported by William and Srawley[3].

Examination of fracture surfaces

The fracture surfaces of DT, SENT and tensile test specimens were examined through scanning electron microscopy (SEM) using a Cambridge Stereoscan 360 and through a Nikon optical microscope. The crack lengths were measured using an optical vernier.

Dynamic mechanical analyses (d.m.a.)

Glass transition temperatures were determined using a DuPont 983 dynamic mechanical analyser at a heating rate of 20°C min^{-1} in resonant mode from −100 to 200°C.

RESULTS AND DISCUSSION

Young's modulus measurements

The variation in Young's modulus with testing rate is shown in *Figure 2*. The modulus increases only slightly with increasing crosshead speed.

Yield stress measurements

The variation in yield stress σ_y with crosshead speed is shown in *Figure 3*. As for the modulus data in *Figure 2*, it is found that the yield stress increases with increasing crosshead speed. Specimens were sectioned after deformation and examined in a polarized-light microscope. The deformation was homogeneous with no evidence of shear band formation. The d.m.a. thermogram of ADC in *Figure 4* exhibits a strong β relaxation which

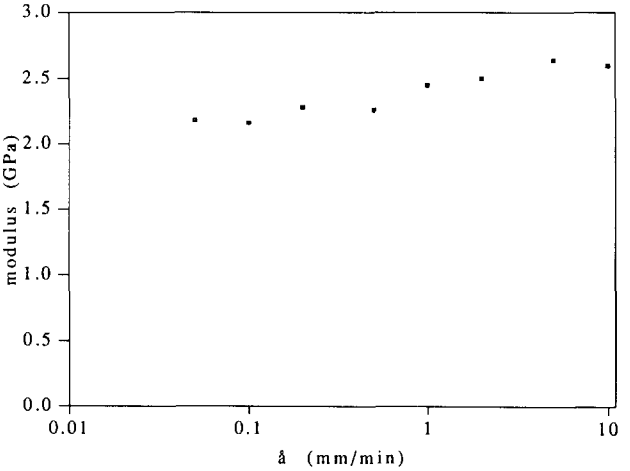

Figure 2 Variation in Young's flexure modulus E with crosshead speed at 20°C for ADC

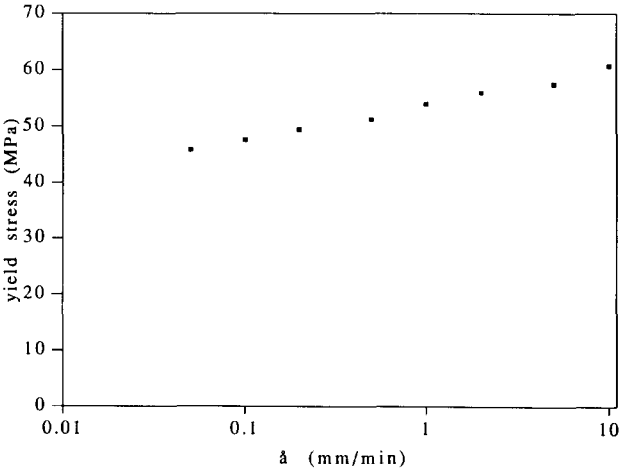

Figure 3 Variation in yield stress σ_y with crosshead speed at 20°C for ADC

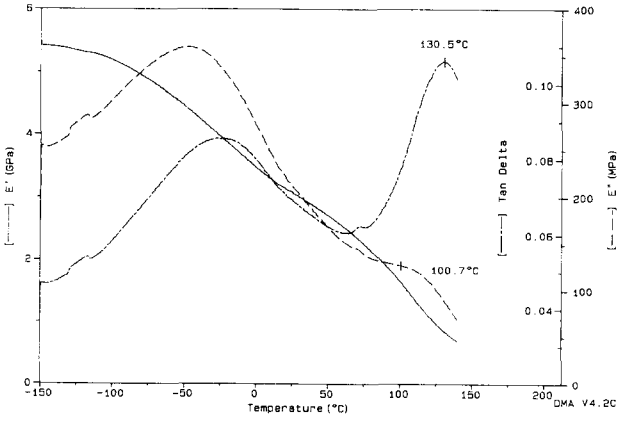

Figure 4 Dynamic mechanical analysis thermogram of ADC

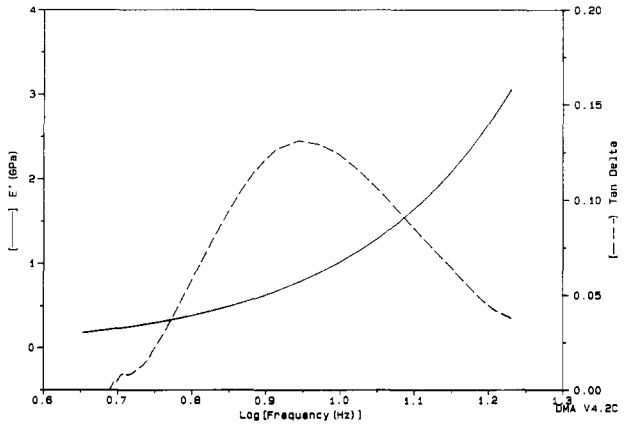

Figure 5 Dynamic mechanical analysis modulus-frequency curve for ADC

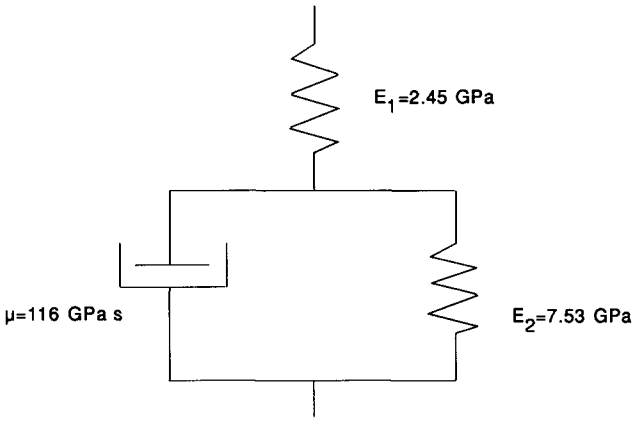

Figure 6 Standard solid model for ADC

extends over a broad temperature range from −50 to 20°C. This influences both the modulus and the yield stress, as reflected in the loading rate dependence of these parameters in *Figures 2* and *3*.

A viscoelastic model for ADC

The viscoelastic behaviour of ADC has been simulated using the standard linear solid model with the elastic moduli E_1 and E_2 and the viscosity η of the viscous element determined for ADC from d.m.a. studies. Mathematical solutions for a sinusoidal loading of a standard linear solid model can be found elsewhere[4]. Using the d.m.a. data presented in *Figure 5* and solving the equations in ref. 4 allowed values of E_1, E_2, and η to be calculated; the results are presented in *Figure 6*.

Fractography

A typical fracture surface of a broken DT test specimen is shown in *Figure 7* at two different magnifications. The surface is characterized by curved crack fronts concentrated at the tension side of the specimen. This type of fracture morphology was identified both in stable and unstable failure mode specimens. The compression side of the specimen was effectively featureless. *Figure 8* shows the fracture surface of an ADC specimen broken in a SENT test. The fracture surface is divided into two distinct regions: a featureless initiation area immediately after the notch, and a 'river markings' region. Long narrow lines run radially from the initiation point, while the major part of the surface is featureless, even at very high magnification. In fracture surfaces of unnotched tensile test specimens, the river markings are less sharp than they are in the SENT test specimens and, as shown in *Figure 9*, flaky patterns are identified in these lines. These may be due to the unnotched tensile stress being an order of magnitude higher than the tensile stress of the notched SENT test specimens. However, examination at high magnification of these flaky patterns did not reveal any evidence of crazing.

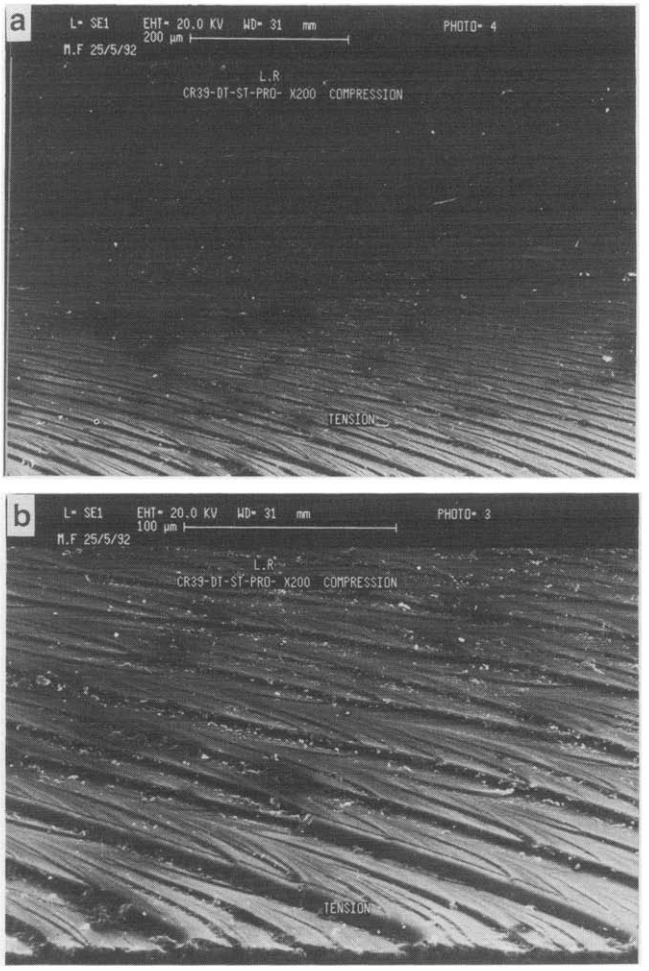

Figure 7 Crack fronts in the double torsion test specimen of ADC: (a) magnification × 160; (b) magnification × 400

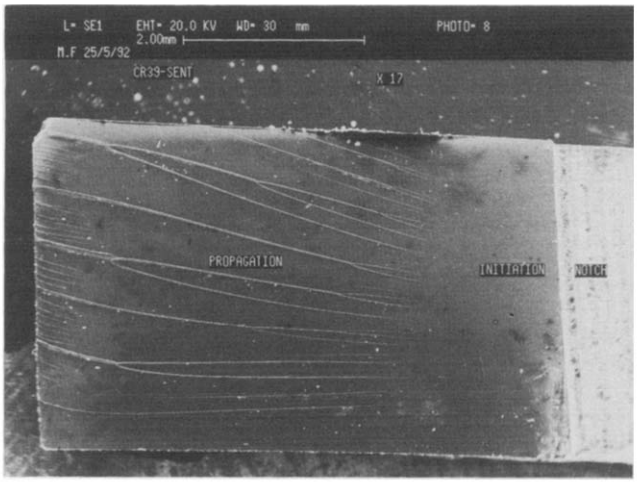

Figure 8 Fracture surfaces in the SENT test specimen of ADC

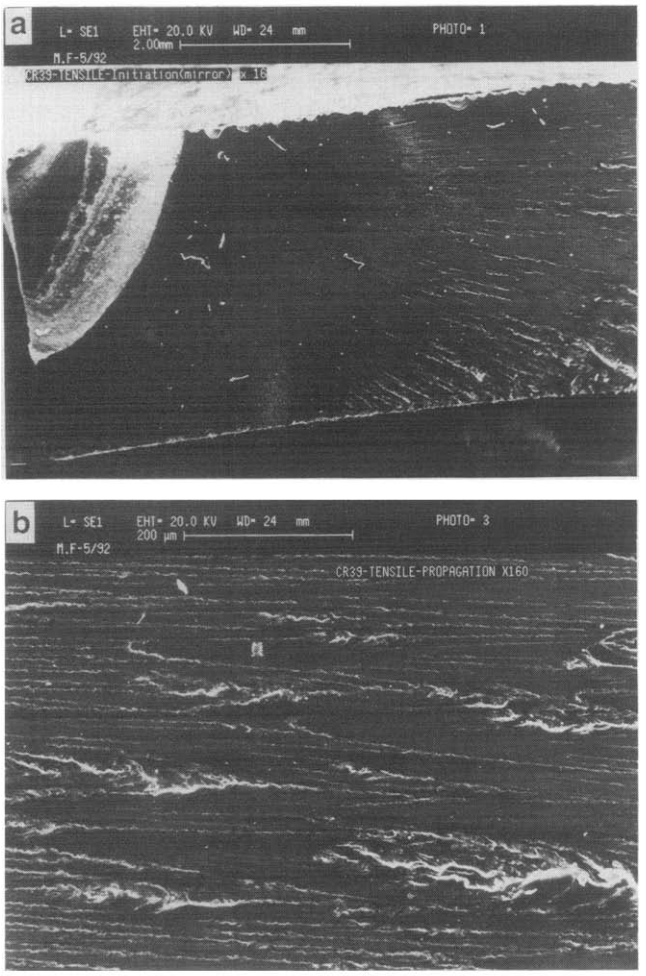

Figure 9 Fracture surface of the unnotched tensile test specimen of ADC: (a) magnification × 16; (b) magnification × 160

Fracture data and mode of crack propagation in ADC

In double torsion tests two types of crack propagation were observed, these being stable or continuous propagation at a constant load after initiation (*Figure 10a*) and unstable or stick-slip propagation (*Figure 10b*), where high amplitude traces are of the sawtooth type, with propagation at a peak load P_i and arrest at the minimum load P_a. These loads correspond to the critical stress intensity factors for initiation (K_{ci}) and arrest (K_{ca}). The differences between the initiation and arrest values of P and K_c characterize the magnitude of the sawtooth. In an effort to understand the mechanism of crack propagation in ADC, tests were conducted at different crosshead speeds and the effect of rate of testing is shown in *Figure 11*. K_{ci} decreases as the crosshead speed increases, whilst K_{ca} remains approximately constant. Thus, as the sawtooth size decreases there is a tendency for a transition to brittle, continuous propagation at high crosshead speeds to occur. The results from SENB tests at varying crosshead speeds show very similar trends in *Figure 12*. In SENB and SENT test pieces, cracks accelerate as soon as they start to propagate. The values of K_c and G_c from three test methods at 1 mm min^{-1} crosshead speed are presented in *Table 1*. The values of G_c were calculated from the equation

$$G_c = \frac{(1-\nu^2)K_c^2}{E} \quad (2)$$

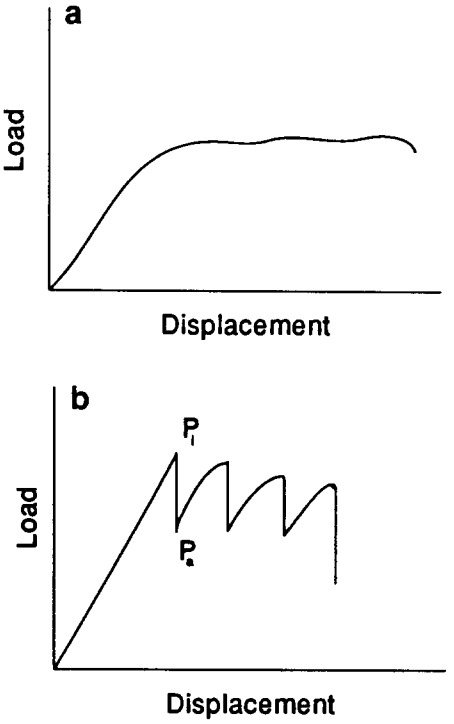

Figure 10 Load–displacement modes in double torsion: (a) stable crack growth; (b) unstable crack growth

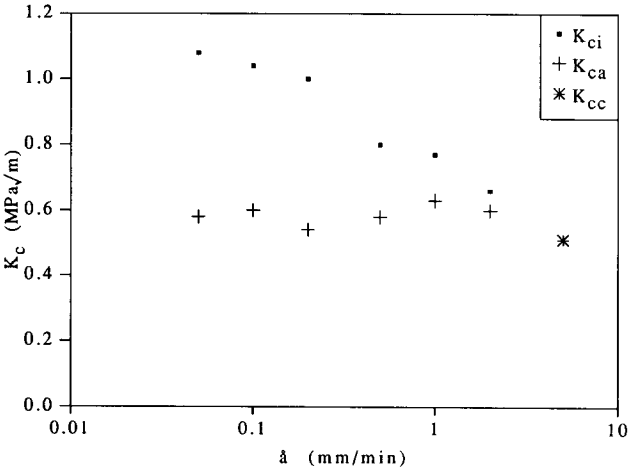

Figure 11 Variation in the critical stress intensity factor K_c with crosshead speed for ADC at 20°C in the double torsion test

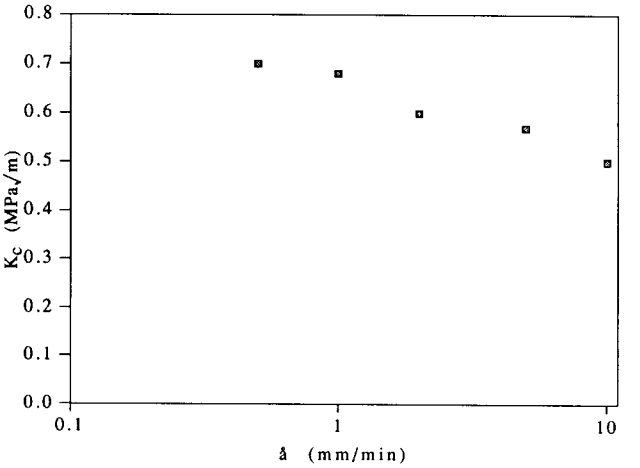

Figure 12 Variation in the critical intensity factor K_c with crosshead speed for ADC at 20°C in the SENB test

Table 1 K_c and G_c values at 20°C for ADC at 1 mm min^{-1}

Testing method	K_c (MPa m$^{1/2}$)	G_c (J m^{-2})
Double torsion (K_{ci})	0.77	347
Double torsion (K_{ca})	0.63	231
Double torsion[a] (K_{cc})	0.51	151
SENB	0.68	270
SENT	0.6	211

[a] The value extrapolated from the data in *Figure 11*

where E is Young's modulus as determined from the previous experiments. The values of G_c lie between 200 and 350 J m^{-2}. The low fracture energies of thermosets compared to thermoplastics are attributed to their crosslinked structures. Although the low value of G_c for ADC indicates that ADC is brittle, the value of G_c is two orders of magnitude higher than the energy required to rupture chemical bonds[5], which is about 1 J m^{-2}. This suggests that even in brittle materials energy dissipation processes such as plastic deformation are occurring under the high strains in the vicinity of the crack tip. It is clear from the SEM studies that there is no evidence of craze debris on the surfaces of the specimens. The crazes in thermoplastics are well defined and may be many micrometres long, whereas crazing has not been generally accepted for thermosets. The yielding behaviour of ADC is said[6] to be identical to that of thermoplastic glassy polymers. Shear yielding is a major energy-absorbing process that does not involve a change in volume of the polymer but requires general cooperative movement of molecular segments[7]. In crosslinked resins, the gross intramolecular motions may be inhibited and shear yielding is highly localized, leading to brittle failure. It has been generally accepted that stick-slip propagation in thermosets can be explained by crack blunting due to crack tip plastic deformation[8]. It is found that if the yield stress σ_y of the resin measured in compression is high then crack growth is continuous, whereas if σ_y falls owing to changes in the test variables, such as rate and temperature, then propagation tends to be stick-slip in nature. This behaviour is shown in *Figure 13*, where K_{ci} is plotted against σ_y measured at various crosshead speeds. A continuous crack propagation suggests very little crack tip plastic deformation, whereas stick-slip behaviour would indicate energy-absorbing deformation at the crack tip. As a result, the higher initiation stress intensity factor K_{ci} may be due to crack blunting, which is controlled by the yield stress of the resin. The stress intensity factor K_{cc} can be correlated[4] to the crack tip radius ρ by the equation

$$\frac{K_{ci}}{K_{cc}} = \frac{(1+\rho/2c)^{3/2}}{(1+\rho/c)} \quad (3)$$

where K_{ci} and K_{cc} are the critical stress intensity factors for a blunt and a sharp crack, respectively. It is postulated that fracture occurs when a critical stress σ_c is reached at a distance c ahead of the crack tip. The crack tip radius can be taken to be equal to the crack tip opening displacement[9] δ and is calculated[10] using the relationship for a Dugdale plastic zone in the crack tip

$$\rho \approx \delta = \frac{K_{ci}^2}{E\sigma_y} \quad (4)$$

The solid line in *Figure 14* is the theoretical relationship between K_{ci}/K_{cc} and $(\rho/2c)^{1/2}$, as predicted by equation (3). The data points in *Figure 14* are fitted to the theoretical curve by choosing an appropriate value of c (this being the only adjustable parameter). The value of the critical distance c used for the data in *Figure 14* was $0.4 \pm 0.02\,\mu$m. Once the value of c has been determined, it is possible to calculate the value of the critical stress σ_c using the relationship[4] $K_{cc} = \sigma_c(2\pi c)^{1/2}$. The value of σ_c for ADC was found to be 320 MPa.

The fact that $\sigma_c/\sigma_y \approx 5$ implies that a stress of the order of $5\sigma_y$ (the yield stress) must be reached in the plastic zone. The critical stress σ_c may be interpreted as a constrained yield stress[7]. The constraint on the plastic zone created by the surrounding elastic material under a plane strain condition could elevate the level of tensile stress σ required for yielding to occur. It has been shown that continuous crack propagation takes place in PMMA when δ, the crack opening displacement, reaches a critical value δ_c, which has a constant value[11,12]. The calculated δ_c values from equation (4) have been plotted in *Figure 15*. As can be seen, with reducing crosshead speed

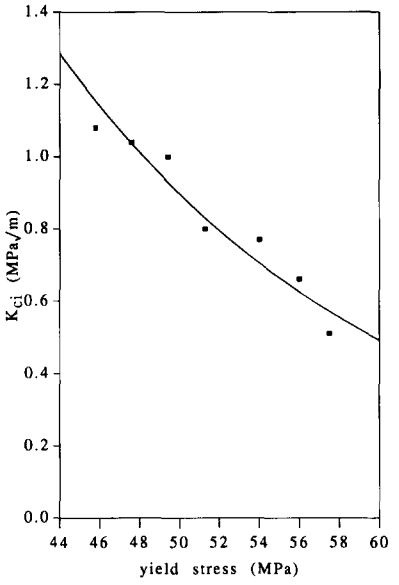

Figure 13 Plot of initiation critical intensity factor K_{ci} against compressive yield stress σ_y for ADC in the DT test at 20°C

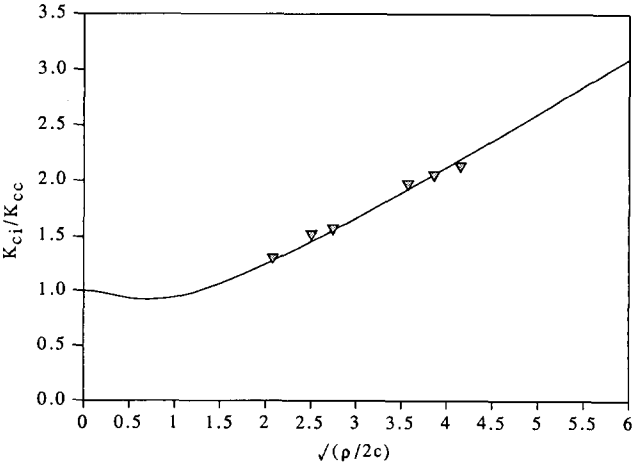

Figure 14 Ratio of initiation critical intensity factor to continuous critical intensity factor (K_{ci}/K_{cc}) as a function of crack tip radius for ADC

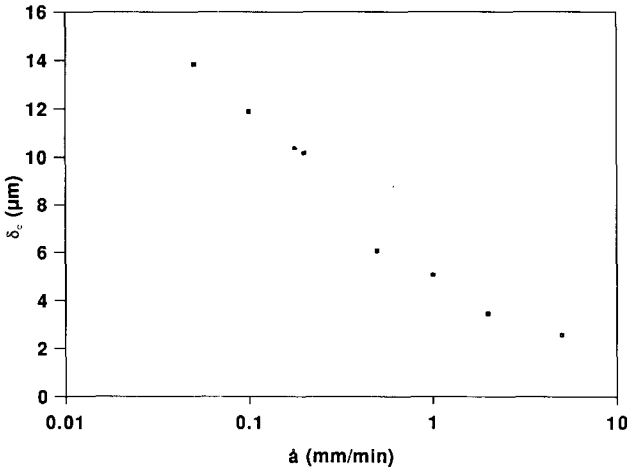

Figure 15 Variation in critical opening displacement δ_c with test rate for ADC

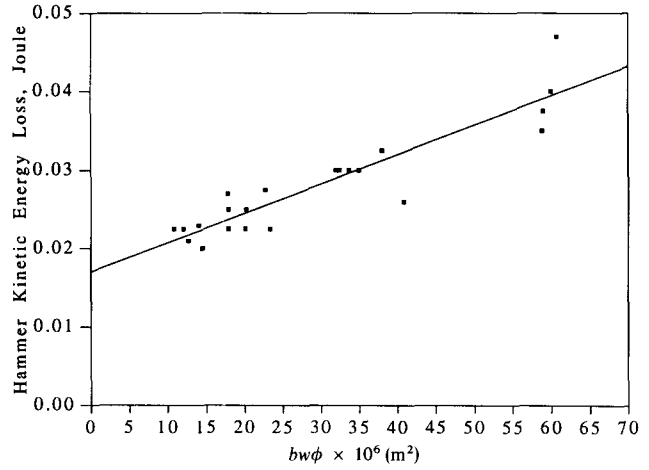

Figure 16 Impact G_c plot for ADC. The plot of hammer kinetic energy loss *versus* $bw\phi$ has a slope of G_c

the value of δ_c rises rapidly, which implies considerable crack tip blunting and stick-slip propagation. The impact critical energy release rate (impact G_c) is obtained from the impact study tests by plotting the equation

$$U_H = G_c bw\phi + U_K \quad (5)$$

where U_H is the hammer energy loss, b is the specimen depth, w is the specimen width, ϕ is the calibration factor function of a/w and the specimen geometry, and U_K is the specimen kinetic energy[10]. The impact G_c for ADC is calculated from the slope of the plot shown in *Figure 16*; G_c is found to be about 350 J m^{-2}. This value represents the fracture energy from a sharp crack.

CONCLUSION

It has been shown that crack propagation behaviour in ADC is controlled by the plastic deformation at the crack tip. The stick-slip propagation, which is more pronounced at low crosshead speeds, has been shown to be caused by a crack-blunting mechanism. No evidence was found for crazing in ADC from optical and electron microscopy investigations. The values of K_c and G_c were found to be about 0.6 MPa m$^{1/2}$ and 0.25 kJ m^{-2}, respectively. These values are of the same order as that expected for crosslinked thermosets. Fracture surfaces are found to be mostly featureless at high magnification, with no indication of crack arrest lines.

ACKNOWLEDGEMENTS

The authors wish to thank Sola International Holdings Research Centre, Adelaide, for the provision of materials and for its support. Mr M. Frounchi would like to thank in particular the Ministry of Higher Education of Iran for the generous provision of a scholarship to undertake this study. We also acknowledge helpful discussions with Dr H. Toh of Sola. The authors also wish to thank the Australian Research Council for their support of this project.

REFERENCES

1 Stevens, H. C., Sare, E. J. and Holtman, M. S. *US Pat. 4 360 653* 1982
2 Evans, A. G. *Int. J. Fract.* 1973, **9**, 267
3 William, F. B. and Srawley, J. E. *ASTM Spec. Tech. Publ.* 1966, No. 410, 12
4 Williams, J. G. 'Stress Analysis of Polymers', Ellis Horwood, London, 1980, pp. 111–117
5 Gleadhill, R. A., Kinloch, A. J., Yamini, S. and Young, R. J. *Polymer* 1978, **19**, 574
6 Frounchi, M., Chaplin, R. P. and Burford, R. P. *Polymer* submitted
7 Kinloch, A. J. and Young, R. J. 'Fracture Behaviour of Polymers', Applied Science, London, 1983, pp. 132–134
8 Phillips, D. C., Scott, J. M. and Jones, M. J. *J. Mater. Sci.* 1978, **13**, 311
9 Kinloch, A. J. and Williams, J. G. *J. Mater. Sci.* 1980, **15**, 987
10 Plati, E. and Williams, J. G. *Polym. Eng. Sci.* 1975, **15**, 470
11 Marshall, G. P., Coutts, L. H. and Williams, J. G. *J. Mater. Sci.* 1974, **9**, 1409
12 Atkins, A. G., Lee, C. S. and Caddell, R. M. *J. Mater. Sci.* 1975, **10**, 1394